Article:
Phadtare, J.A., Fletcher, J.K., Ross, A.N. et al. (Cover date: October 2023 Part B) Unravelling the Mechanism of Summer Monsoon Rainfall Modes over the West Coast of India using Model Simulations. Quarterly Journal of the Royal Meteorological Society, 149 (757). pp. 3164-3182. ISSN: 0035-9009

https://doi.org/10.1002/qj.4550

ORIGINAL ARTICLE

Unravelling the Mechanism of Summer Monsoon Rainfall Modes over the West Coast of India using Model Simulations

Jayesh A. Phadtare[1,2*] | Jennifer K. Fletcher[1,2] | Andrew N. Ross[1] | Andrew G. Turner[3,4] | Reinhard K. H. Schiemann[4] | Helen L. Burns[5]

[1]School of Earth and Environment, University of Leeds, UK

[2]National Centre for Atmospheric Science, University of Leeds, UK

[3]Department of Meteorology, University of Reading, UK

[4]National Centre for Atmospheric Science, University of Reading, UK

[5]Centre for Environmental Modelling And Computation, University of Leeds, UK

Correspondence
Jayesh Phadtare, Department of Civil and Environmental Engineering and Earth Sciences, University of Notre Dame, Notre Dame, IN 46556
Email: jayesh.phadtare@gmail.com

Present address
*Department of Civil and Environmental Engineering and Earth Sciences, University of Notre Dame, Notre Dame, IN 46556

Funding information
Weather and Climate Science for Service Partnership (WCSSP) India, a collaborative initiative between the Met Office, supported by the UK Government's Newton Fund, and the Indian Ministry of Earth Sciences (MoES).

A transition from a predominantly offshore to an onshore rainfall phase over the west coast of India was simulated using three one-way nested domains with 12-, 4-, and 1.33-km horizontal grid spacing in the Weather Research and Forecasting model. The mechanism of offshore-onshore rainfall oscillation and the orographic effects of the Western Ghats are studied. A convective parameterization scheme was employed only in the 12-km domain. A trough extending offshore from the west coast facilitates offshore rainfall. This trough is absent during the onshore phase, and rainfall occurs over the coast mainly via orographic uplift by the Western Ghats. The model overestimates rainfall over the Western Ghats at all resolutions as it consistently underestimates the boundary layer stratification along the coast. Weaker stratification weakens the blocking effect of the Western Ghats, resulting in anomalous deep convection and rainfall over its windward slopes. The 4- and 1.33-km domains simulate the offshore-to-onshore transition of rainfall but fail to capture a sufficient contrast in rainfall between land and sea compared to observations. The 12-km domain produces light rainfall, anchored along the coast, throughout the simulation period, and hence gravely underestimates the offshore rainfall. The offshore rainfall persisted in the 4- and 1.33-

km domains in a sensitivity experiment in which the Western Ghats were flattened. This suggests that orographic effects do not significantly influence offshore rainfall. In another experiment, the convective parameterization scheme in the 12-km domain was turned off. This experiment simulated the offshore and onshore rainfall phases correctly to some extent but the rainfall intensity was unrealistically high. Thus, a model with a horizontal grid spacing of O($\sim$ 1 km), in which convection evolves explicitly, is desired for simulating the west coast rainfall variations. However, improvements in the representation of boundary layer processes are needed to capture the land-sea contrast.

KEYWORDS
Orographic effects, Indian Summer monsoon, Coastal rainfall

1 | INTRODUCTION

The west coast of the Indian peninsula is one of the rainiest places on our planet and a host to rainforests with a high level of biodiversity, thanks to the Western Ghats mountain range. This region is prone to flash floods and landslides during the summer monsoon season (Francis and Gadgil, 2006; Kumar et al., 2008; Hunt and Menon, 2020; Mohandas et al., 2020). In June 2016, the Interaction of Convective Organization and Monsoon Precipitation, Atmosphere, Surface and Sea (INCOMPASS) field campaign took place over the Indian region in order to understand the interaction between the convective and large-scale weather systems in the summer monsoon (Turner et al., 2020). One of its southern legs involved aircraft and ground-based observations over the west coast of India and the adjacent Arabian Sea during 21-26 June (henceforth referred to as the 'INCOMPASS IOP'). Heavy rainfall shifted from the offshore region (henceforth referred to as the 'offshore mode') to the onshore region (henceforth referred to as the 'onshore mode') during this period. It was speculated that the interactions between the monsoonal westerly jet, a mid-tropospheric dry air intrusion, and convection lead to the offshore and onshore rainfall modes (Fletcher et al., 2020). A climatological study by Hunt et al. (2021) supports this hypothesis. Grossman and Durran (1984), with the help of field observations and a simple 2D model of flow over an orographic barrier, suggest that the offshore rainfall over the Arabian Sea may result from upstream blocking and uplift of the monsoonal jet by the Western Ghats. On the other hand, a study involving WRF model simulations by Zhang and Smith (2018) suggests that the offshore rainfall results from large-scale instabilities, and that the Western Ghats merely serve as the eastern boundary for it. Shige et al. (2017) and Hunt et al. (2021) showed that the offshore-onshore oscillation of rainfall over the Indian west coast is associated with large-scale forcing from the Boreal Summer Intraseasonal Oscillation (BSISO) phases.

Current operational numerical weather models still have issues in realistically simulating rainfall over this coastal hilly region. A 10-day weather forecasting exercise in support of the INCOMPASS field campaign showed that the operational Met Office Unified Model (MetUM) at a horizontal resolution of N768 (17 km) with a convection scheme, as well as its limited-area model (LAM) version at 4.4 km using explicit convection, overestimate the onshore rainfall and underestimate the offshore rainfall over the west coast (figure 10 in Martin et al. (2020)); this could be a direct consequence of poor representation of the offshore-onshore rainfall modes. Mohandas et al. (2020) reported that medium-range forecasts from the global National Centre for Medium-Range Weather Forecasting (NCMRWF) Unified Model (NCUM), a version of MetUM, simulate the observed

circulation patterns over the west coast but do not get the rainfall distribution right. Rajendran et al. (2012) argues that capturing the convective-regional-global scale interaction is necessary in order to simulate the observed long-term rainfall trends over this region in the models. Thus, a realistic simulation of offshore-onshore rainfall modes over the west coast and their relationship with large-scale weather systems is imperative for regional and global models in order to produce useful short-term and long-term forecasts of rainfall.

Smith et al. (2015) show that the MetUM simulates the observed rainfall intensity over the hills on the west coast of the UK at 1.5 km resolution; rainfall intensity reduces when the resolution is decreased. They suggest that the sensitivity of the orographic rainfall to the horizontal grid spacing is different for different mountain ranges and it is mainly governed by the geometry of the orographic features. In general, the horizontal grid spacing that is adequate to faithfully represent the effects of orography on simulated rainfall appears to be a few to 10 km (see Smith et al. (2015) and references therein). Some of the latest operational numerical weather prediction (NWP) models employ grid spacing of O($\sim$ 1 km). The fundamental assumption in the convective parameterization is that the convective cells are much smaller than the model grid box and remain unresolved. At O($\sim$ 1 km) resolution, convective cells are partially resolved. Thus, the usage of a convective parameterization scheme at this resolution is questionable as individual convective cells can occupy more than one grid box. This scale is generally referred to as the 'grey zone' of convective parameterization (Gerard et al., 2009; Kirshbaum, 2020). Peatman et al. (2014) showed that the models which rely on convective parameterization fail to simulate the observed interaction between convection and sea breeze over the islands of the Maritime Continent. High-resolution convection-permitting simulations produced a much improved diurnal cycle of circulation and rainfall (Birch et al., 2015, 2016). Nevertheless, there are many studies where the usage of a convective parameterization scheme within and near the grey zone of convection has improved the overall model simulation of a meteorological event (e.g., Zheng et al. (2016); Mahoney (2016); Phadtare (2018)). This can be due to the prescribed CAPE consumption and entrainment-detrainment rates for shallow and deep convection in the scheme. Recently, convective schemes are being improved by including a scale-dependency in these factors (e.g. Zheng et al. (2016)).

The grid spacing of a few km, however, is inadequate to resolve the eddies within the planetary boundary layer (PBL). Thus, a PBL scheme is needed to represent the boundary layer processes (Wyngaard, 2004; Honnert, 2016; Kirshbaum, 2020). The boundary layer processes determine the orographic influence by controlling the near-surface stratification of the atmosphere. One of the key parameters controlling the orographic effects is the Froude Number (F) of the impinging flow:

$$F = \frac{U}{N H} \tag{1}$$

where U is the mean wind speed upstream of the orographic barrier, N is the mean Brunt-Väisälä frequency of the atmosphere, and H is the height of the orography (Sheppard, 1956; Smith, 1979; Kirshbaum et al., 2018). When F < 1, flow is blocked by the orographic barrier, whereas when F > 1, the flow has sufficient kinetic energy to overcome the orographic barrier and move to the lee side. Several idealized simulation experiments (Chu and Lin, 2000; Chen and Lin, 2005b,a; Jiang, 2003; Reeves and Lin, 2007; Miglietta and Rotunno, 2009) have shown that in the blocked case, precipitating systems remain upstream of the orography, and in the unblocked case, precipitation occurs over the orographic slopes (heavy) and the lee region (light to moderate). A recent study by Phadtare et al. (2022) showed that when the incident low-level flow over the west coast of India is classified according to F, the classification leads to the offshore-onshore rainfall pattern – the low F values are associated with the offshore mode, and high F values with the onshore mode. Further, they show that the offshore mode is characterised by strong land-sea breeze variations and greater control of the local diurnal cycle over the west coast rainfall. Conversely, the onshore mode has suppressed land-sea breeze and the rainfall has a weak diurnal cycle. Thus, the mechanisms by which the release of convective instability takes place in the two modes are different. Mechanical uplifting is dominant during the onshore mode, whereas during the offshore mode, it is mainly facilitated by daytime heating. Therefore, even though the majority of the literature suggests that

the offshore-onshore modes are caused by the large-scale variability of the atmosphere, the blocking/uplifting from the Western Ghats, as well as its thermal forcing, seem to play an important role. Thus, a pertinent question that needs to be answered is: are the representation of orographic effects and the diurnal cycle of rainfall in the present-day models adequate for simulating the offshore-onshore rainfall modes?

The purpose of this study is to understand the impacts of horizontal grid resolution and the presence of a convective parameterization scheme on the model simulation of the offshore-onshore rainfall modes over the west coast of India and understand the role of the Western Ghats in these modes. The INCOMPASS IOP is chosen as a case study. Section 2 of this article describes the datasets used and model setup, section 3 shows how model domains at different horizontal resolutions perform at simulating the observed offshore-onshore rainfall transition and the evolution of dynamics, section 4 presents the results of model sensitivity experiments relating to the convective parameterization and the presence of the Western Ghats. Section 5 presents the main conclusions and discussion on the future avenues for research.

2 | DATA AND MODEL SETUP

2.1 | IMERG rainfall

The Integrated Multi-satellitE Retrievals for GPM (IMERG) product, version 06B (Huffman et al., 2015), is used for describing the patterns of rainfall over the Indian west coast during the offshore-onshore modes. IMERG provides global surface rainfall on a 0.1° spatial grid at 30-minute intervals. The dataset is provided by the National Aeronautics and Space Administration (NASA). IMERG is produced by merging passive microwave and infrared rainfall estimates which are further calibrated with the rain gauges on a monthly basis. Satellite-based rainfall estimates over the west coast of India are known to have biases. The Tropical Rainfall Measuring Mission (TRMM) 3B42 product gives the maximum rainfall off the coast instead of the Western Ghats slopes. This is because the coastal clouds are deeper than those over the Western Ghats (Shrestha et al., 2015; Kumar and Bhat, 2017), and hence the infrared rainfall estimates undervalue the orographic rainfall. The latest IMERG product places the maximum rainfall correctly over the Western Ghats slopes (e.g., Prakash and Srinivasan (2021); Phadtare et al. (2022)), but still underestimates the intensity of heavy rainfall episodes (> 25 mm h^{-1}) compared to the rain gauges (Murali Krishna et al., 2017). Rojas et al. (2021) concluded that IMERG underestimated the overall rainfall over the mountainous region of Chile by 16% and warm rain events by 50%. Thus, it is possible that the IMERG underestimates the actual rainfall over the orography of the Western Ghats by about 16-50%.

2.2 | Rain gauges

To validate the IMERG rainfall, we have used rainfall data from the rain gauge network of the India Meteorological Department (IMD). The network comprises automatic weather stations (AWS) and automatic rain gauges (ARG) (Saha et al., 2021). These automatic stations use tipping-bucket rain gauges. The dataset was obtained from IMD in support of the Indo-UK joint INCOMPASS project. A total of 44 rain gauges were selected along the west coast. Rain gauges with more than 10% missing data were excluded from the analysis.

2.3 | Radiosondes

We use the upper-air radiosonde observations from Mangalore (74.83°E, 12.95°N and 31 m elevation) and Amini Divi (72.73°E, 11.12°N and 4 m elevation) stations in order to evaluate the model simulation for the near-surface stratification and winds. This data was obtained from the Atmospheric Soundings web portal of the University of Wyoming (`weather.uwyo.edu/upperair/`

sounding.html). Mangalore is located over the west coast, whereas Amini Divi is an island in the Arabian Sea. Radiosonde observations are ideal for determining the near-surface stratification as they provide high-resolution in situ observations. The near-surface atmospheric stratification directly influences the orographic blocking as well as the sub-grid orographic drag parameterization (Stensrud, 2009).

2.4 | Reanalysis

The fifth-generation European Centre for Medium-Range Weather Forecasts Reanalysis (ERA5) dataset is used for evaluating the model simulated large-scale fields. ERA5 is available at hourly intervals on a 0.25° horizontal grid and 137 vertical levels starting from the surface and up to a height of 80 km (Hersbach et al., 2018).

2.5 | WRF model

The Advanced Research version of the Weather Research and Forecasting (WRF 4.1.3) model (Skamarock et al., 2008) is used to simulate the INCOMPASS IOP. Three one-way nested grids, all centred over the Indian west coast, were employed for the simulations (Fig. 1). The outermost grid will be referred to as D12, the intermediate as D4, and the innermost as D1 as the grid spacings of these domains are 12, 4, and 1.33 km, respectively. D12 is large enough to include the entire Arabian Sea to the west, the Bay of Bengal to the east and the Himalayas to the north. D1 is large enough to include the entire Western Ghats over the Indian peninsula and the mesoscale systems over the offshore region of the Arabian Sea. The physics schemes recommended in the tropical suite of the WRF model are used. The modified Tiedtke convective parameterization scheme (Tiedtke, 1989; Zhang et al., 2011) is used only in D12. This scheme accounts for deep, middle, and shallow convection. The domains D4 and D1 allow convection to develop explicitly. More details on the grids used and other physics schemes are given in Table 1. 35 vertical eta levels are used with a lid at 50 hPa; the lowest level is at 20 m elevation above the surface and there are 10 levels below 1500 m. Note that one-way nesting was used here in order to understand the differences in the simulation of each domain. In two-way nesting, the inner/finer domain gets the boundary conditions from the outer/coarser domain, and the output of the inner domain is fed back to the outer grid to improve the overall simulation; in one-way nesting, only the former part is true. The initial and lateral boundary conditions to D12 are taken from ERA5.

Each mode of the offshore-onshore rainfall oscillation can last for about 4-7 days (Fletcher et al., 2020; Hunt et al., 2021). Thus, in order to allow sufficient time for such variability to develop in the model simulation, we start the simulation at 0000 UTC 13 June 2016 and end it on 0000 UTC 28 June 2016; only the simulation between 0000 UTC 20 June - 0000 UTC 28 June, a period which coincides with the INCOMPASS IOP, is analyzed.

3 | CONTROL SIMULATION

The purpose of the control simulation is to simulate the event as realistically as possible using actual topographical and meteorological conditions as input. Model biases in the simulated rainfall and other meteorological parameters are identified for all domains in this run. The sensitivity simulations described in section 4 will be compared with the control run in order to understand the effect of the modified topography and convection representation in the model.

Domains	D12	D4	D1
Grid cells	356×348	649×601	889×985
Grid spacing	12 km	4 km	1.33 km
Boundary conditions	ERA5	D12	D4
Convection	New Tiedke (Tiedtke, 1989; Zhang et al., 2011)	-	-
Microphysics	WRF Single-moment 6-class (Hong and Lim, 2006)		
Planetary boundary layer	Yonsei University (Hong et al., 2006)		
Surface layer	MM5 (Zhang and Anthes, 1982)		
Land surface	Noah (Chen and Dudhia, 2001)		
Radiation	RRTMG (Iacono et al., 2008)		

TABLE 1 Details of the WRF domains shown in Figure 1 and the physics schemes used.

3.1 | Rainfall

First, we identify the offshore and onshore modes of rainfall, if they exist, in different domains of the model. The model evaluation can then be done on the basis of the time periods of these modes, and the overall distribution and the diurnal cycle of rainfall in each mode.

3.1.1 | Offshore and onshore modes

Figure 2 shows Hovmöller diagrams of 12-14°N mean rainfall during 20-27 June from the IMERG rainfall product and the three WRF domains. The latitudinal band of 12-14°N is chosen as this was the region where the INCOMPASS IOP was conducted and the transition of rainfall from offshore-to-onshore region was seen (Fletcher et al., 2020). Rainfall occurs over the offshore region during 20-24 June ('Offshore' mode), and over the onshore region ('Onshore' mode) during 26-27 June; the offshore region gets little rainfall during the onshore mode (Fig. 2a). Domains D4 and D1 simulate the offshore and onshore modes of rainfall somewhat similar to the observed modes (Fig. 2c,d). Distinct offshore and onshore modes are not seen in domain D12, which employs a convection scheme (Fig. 2b). According to the IMERG observations, the offshore mode is characterized by rainfall episodes occurring in the early morning hours over the sea, and the onshore mode by a stationary system over the coast and the Western Ghats. Domains D4 and D1 qualitatively simulate these characteristics of offshore and onshore modes. However, note that during the offshore mode, the intensity of rainfall over the coast in these domains is much greater than observed.

3.1.2 | Mean rainfall

In IMERG, two prominent offshore rainfall zones are seen during the offshore mode, a northwest-southeast oriented rain band over the Arabian Sea and an off-the-coast rain band (Figure 3). Heavy rainfall (> 30 mm/day) is widespread over the sea while rainfall is mostly light over the coast. During the onshore mode, rainfall around Mangalore increases (>50 mm/day), with the slopes of the Western Ghats at 14°N receiving the heaviest rainfall (> 80 mm/day). Note that the onshore mode is seen only to the south of 15°N in this case. An Offshore rainband is seen north of 15°N. A clear land-sea contrast in rainfall is quite evident during both modes in the 12-14°N belt. In domain D12, rainfall is located along the coast during both modes. Domains D4 and D1 do get the offshore and onshore modes right to some extent. Although there is heavy rainfall over the sea during the

offshore mode in these domains, it is not located as far offshore as in the IMERG field. In addition, there is heavy rainfall (> 80 mm/day) over the coast during the offshore mode and the observed land-sea contrast in rainfall is missing in D4 and D1. During the onshore mode, heavy rainfall in domains D4 and D1 is mainly over the Western Ghats slopes. In these domains, the coastal region receives only light rainfall during this mode. In reality, a broad patch of heavy rainfall accumulation, extending from the Western Ghats slopes to the coastal zone, is seen in the IMERG field during the onshore mode. Thus, although the convection-permitting domains simulate the offshore and onshore rainfall during the respective modes, it is erroneously shifted eastwards, i.e., towards the orography. This discrepancy is further emphasized in the next figure.

Figure 4 shows rainfall anomalies in the WRF domains with respect to the IMERG rainfall. The rainfall fields in these domains are regridded to the IMERG resolution for ease of comparison. The anomalous rainfall intensity over the west coast during the offshore mode is between 50-100 mm day^{-1} which is far higher than the reported underestimation of orographic rainfall by the IMERG product (16-50%). During the onshore mode, D12 gravely underestimates the west coast rainfall. The D4 and D1 overestimate rainfall over the Western Ghats slopes by 50-100 mm day^{-1} at most places and slightly underestimate rainfall along the coast south of 15°N where the onshore mode is seen.

3.1.3 | Diurnal cycle

Phadtare et al. (2022) showed that the rainfall during the offshore regime is controlled by a strong diurnal cycle, whereas that during the onshore regime has a weak diurnal cycle. Therefore, here we analyze if the model can simulate the observed diurnal cycle of rainfall during the offshore mode. Figure 5 shows the diurnal variation of mean rainfall over a latitudinal band of 12-14°N during the offshore mode of this case study from IMERG and model simulations. Just off the coast, the IMERG rainfall increases in the early morning period of 0000-0300 UTC (0530-0830 IST), and during 0300-0600 UTC rainfall increases further offshore. The D4 and D1 domains simulate the near-coast heavy rainfall mode during 0000-0300 UTC correctly but miss the enhancement further offshore during 0300-0600 UTC. Notice that the early morning rainfall in IMERG stays strictly off the coast (Fig. 5a), whereas the simulated offshore rainfall in D4 and D1 intrudes over the land. These domains also simulate onshore rainfall maxima during 0600-1200 UTC. Onshore daytime rainfall is not seen at all in the IMERG dataset. Thus, anomalous morning, as well as daytime rainfall over land in D4 and D1, lead to anomalous rainfall over the coast during the offshore mode. In domain D12, offshore rainfall increases during 0000-0600 UTC but the intensity remains less than half of the observed intensity. Rainfall over the coast increases around 0400 UTC and remains high throughout the day.

To summarize, the west coast rainfall modes are entirely absent in D12; the rainfall is anchored along the coast almost all the time and offshore rainfall is very weak in this domain. The D4 and D1 domains do simulate the offshore-onshore modes, but they fail to capture the land-sea contrast and the diurnal cycle of rainfall along the coast during the offshore phase. Both domains produce daytime maximum rainfall over land which is not seen in the observations.

3.2 | Dynamics and thermodynamics

This section evaluates the model simulation for its dynamic (synoptic, mesoscale) and thermodynamic (humidity, convection) fields. In the process, explanations for the discrepancies in the simulated rainfall fields reported in section 3.1 are given.

3.2.1 | Large-scale dynamics

During the offshore mode, there was a northwest-southeast oriented trough over the region extending from the northern Arabian Sea to the southern Bay of Bengal. Note that the rainfall over the Arabian Sea occurs over the trough region with its limits being a ridge to the west and the Western Ghats to the east (Figures 2a, 3a). During the onshore mode, the trough over the Bay of

Bengal moved northeastwards and transformed into a well-developed cyclonic circulation. The western end over the northern Arabian Sea also intensified and developed into a closed cyclonic circulation. A ridge sits over the west coast during this mode which provides an unfavourable environment for the organised large-scale rainfall. However, the westerly jet is stronger during this mode and rainfall over the west coast mainly results from the orographic lifting (Phadtare et al., 2022). Note that the offshore mode is not the same as the break phase (Krishnan et al., 2000) of the summer monsoon. Organized rainbands are absent over the Indian region during the break phase, but they do appear over the eastern Arabian Sea during the offshore phase. However, the offshore-onshore mode oscillation is likely to happen during the break-to-active transition as organized rainbands propagate northward (Shige et al., 2017; Hunt et al., 2021). The model simulates the main features of the offshore and onshore modes correctly (Figure 6b,d), but overestimates the wind speed, especially downstream of the Western Ghats, i.e. over the Indian peninsula and the Bay of Bengal, during the onshore mode. This wind bias is also seen in the D4 and D1 domains (not shown).

The offshore rainfall not only cools the boundary layer over the sea, but the cold pools also present a substantial barrier to the low-level monsoonal flow. Figure 7 shows 950 hPa virtual potential temperature perturbation and winds during the simulated rainfall events in the offshore and onshore modes from domain D1. During the offshore event (Fig. 7a) the rainfall has a squall-line-like north-south organization. This system was propagating westward (Fig. 2d) and it leaves a trail of cold air behind it. The low-level monsoonal flow is obstructed by this cold pool, and the outflow itself is directed southward. As a consequence, the flow along the coast is cooler and has a northwesterly direction leading to suppression of rainfall over the coast. On the other hand, during the onshore mode (Fig. 7b), the flow is westerly and almost perpendicular to the Western Ghats. The air parcels reaching the coast during the onshore event are warmer than those during the offshore events by about 2-3 K. As a result, rainfall is enhanced over the Western Ghats. These simulated features of offshore and onshore rainfall events are in accordance with the observations of Fletcher et al. (2020). The onshore mode is also characterized by a drier mid-troposphere and moister lower-troposphere over the Arabian Sea (Fletcher et al., 2020; Hunt et al., 2021). The simulated humidity fields in the three domains are analyzed next.

3.2.2 | Mid-tropospheric humidity

Figure 8 shows the difference in the vertical cross-section of specific humidity averaged over the 12-14°N band during the onshore and offshore modes in the three model domains. All domains simulate a drier mid-troposphere and moister lower-troposphere during the onshore mode. The westerlies are also stronger during the onshore mode. However, note that in domain D12, the onshore winds do not strengthen and the Western Ghats slopes are drier during the onshore mode compared to the offshore mode. This is contrary to the observations of the case study (Fletcher et al., 2020) and this is the reason that the Western Ghats receive less rainfall during the onshore mode than the offshore mode in D12 (Figure 4). In domains D4 and D1, the low-level wind and moisture anomalies during the onshore mode are strongest over the west coast. This leads to rainfall enhancement over the Western Ghats slopes during the onshore mode.

3.2.3 | Convection

Figure 9 shows the vertical cross-sections of the temporal fraction for which the simulated radar reflectivity was at least 20 dBZ in any grid-box in the 12-14°N latitudinal band in the D4 and D1 model domains. The 20 dBZ threshold is typically used to identify precipitation features in a radar dataset, e.g., Xu and Rutledge (2015). In D12 domain, the convective rain is a subgrid entity produced by the convective parameterization scheme, and it is not reflected in the grid-resolved hydrometeor fields (Chen et al., 2021). Therefore, simulated radar reflectivity from domain D12 is not shown. In domains D4 and D1, there is a frequent widespread deep convection over the Arabian Sea and the west coast during the offshore mode. During the onshore mode, convection is less frequent and remains below 2.5 km altitude over the Arabian Sea. During this mode, deep convection is

confined to the coast. The simulated transformation in the deep convective activity in D4 and D1 is similar to that reported by Fletcher et al. (2020) and Hunt et al. (2021). The only difference is that the model domains simulate deep convection over the coast and orography even during the offshore mode, whereas in the observations it occurred only over the sea. This suggests that there is an anomalous supply of conditional instability to the coast during the offshore mode in D4 and D1. Notice that the dry air intrusion spans the entire region during the onshore mode and not just the offshore part (Fig. 8). Nevertheless, deep convection develops over the coast. This suggests that if the low-level supply of conditional instability and an uplifting mechanism (orography in this case) are present, deep convection can develop despite a dry mid-troposphere.

3.2.4 | Orographic blocking

The model simulates warmer and weakly stratified PBL over the coast during both modes compared to the radiosonde observations (Figure 10a,e). The nighttime temperature anomaly at the surface is around 4 K during the onshore mode. The anomaly reduces in the daytime to around 2 K. Thus, the model severely underestimates the nocturnal cooling of the surface and PBL. The zonal wind speed profiles from the radiosondes (Figure 10b,f) show a stronger monsoonal jet during the onshore mode than the offshore mode. The model captures this variation, however, it overestimates wind speed below 800 hPa at both times. The 0000 UTC equivalent potential temperatures (θ_e) are also higher (by 7-10 K) in the PBL, suggesting that the model transports more instability towards the Western Ghats during nighttime (Figure 10c). During the daytime, the PBL warms up; the simulated θ_e values are closer to the observations at 1200 UTC (Figure 10g). Due to the warmer temperatures, the relative humidity in the PBL is also lower in the simulation compared to the observations (Figures 10d,h). Profiles from the D12 and D4 domains also exhibit similar PBL biases over but they are not shown for the sake of brevity.

The radiosonde profile during the onshore mode shows a well-mixed PBL over the Arabian Sea, whereas the offshore mode has a stratified PBL (Figure 10i). The PBL stratification may be due to the evaporative cold pools produced by the rainfall. Since rainfall is absent over the offshore region during the onshore mode, the offshore PBL is well mixed. The model consistently produces a well-mixed PBL irrespective of the rainfall mode. It simulates the wind speed within the PBL correctly but overestimates the jet speed at 800 hPa by about 4-5 $\mathrm{m\,s^{-1}}$.

As a result of the bias towards stronger wind and weaker PBL stratification, the orographic blocking is weak in the model. Figure 11a-c shows U, N, and F values, respectively, averaged over 50-1000 m altitude above the surface (refer to equation 1) from the 0000 and 1200 UTC Mangalore radiosondes and the corresponding values of these parameters from the hourly output of the WRF simulation. The simulated soundings are averaged over a 12 km horizontal box centred over the radiosonde location. The mean height of the Western Ghats within the 12-14°N band is considered for H, which is about 1000 m. The Western Ghats range is roughly oriented in the north-south direction, therefore the zonal wind speed is considered for U. The effect of saturation during the ascent on the stratification (N) is neglected. Note that ideally, F should be calculated away from the orography using the upstream undisturbed values of U and N. The blocking distance of the Western Ghats extends offshore by 150-300 km (Phadtare et al., 2022). Mangalore is well within the blocking region of the Western Ghats. Therefore, the flow at Mangalore is already decelerated due to the orographic blocking and the F calculated here will be an underestimation of the actual F values. On the other hand, in the precipitating environment, offshore stratification is weaker than coastal stratification due to the piling up of cold pools over the mountain slopes (Phadtare, 2018). This is evident in figures 10a,l during the onshore mode. Therefore, the F values calculated from the offshore sounding will be an overestimation of the actual F values. Amini Divi is an island station (Figure 1) located around 300 km offshore from the Western Ghats, i.e., away from its blocking distance. Figure 11d-f shows U, N, and F values, respectively, averaged over 50-1000 m altitude above the surface from the 0000 UTC Amini Divi radiosondes and the corresponding values of these parameters from the hourly output of the WRF simulation; the 1200 UTC radiosondes were not released from Amini Divi during this period.

Given these limitations in estimating the true F of the flow impinging on the Western Ghats, we avoid the terms ‘blocked’ or

'unblocked' in describing its regime. Instead, phrases like 'weakly blocked'/'strongly blocked' are used. The main aim of this exercise is to show the difference in the observed and simulated flow blocking. The model overestimates U and underestimates N most of the time at the coast, and hence, overestimates F of the flow implying weaker orographic blocking. According to the Mangalore (Amini Divi) radiosonde observations, the F values at 000 UTC hover around 0.5 (1) during the offshore mode. After 26 June, F values are higher and stay between 0.7-1 (2-5) at Mangalore (Amini Divi). The true F of the flow may lie between the F values calculated from the Mangalore and Amini Divi soundings. In D4 and D1 domains, F values are 2-3 times higher than the observed values at Mangalore. During the offshore mode, the simulated F values greater than 1 (2) are consistently seen at Mangalore (Amini Divi). This suggests that the onshore flow in the model is weakly blocked, instead of strongly blocked as suggested by the radiosondes.

In summary, stronger winds, weaker PBL stratification, and hence weakly blocked onshore flow lead to enhanced orographic lifting in the model. Stronger and warmer onshore flow also allows a greater supply of instability towards the orographic slopes. Therefore, the model tends to simulate stronger convection (Fig. 9) and higher rainfall (Fig. 3, 4) over the slopes of the Western Ghats, even during the offshore mode.

4 | SENSITIVITY EXPERIMENTS

This section investigates the sensitivity of the simulated west coast rainfall modes to the orographic influence and mesoscale convective processes in the model. Section 3.2.4 showed that the orographic blocking is weak in the model compared to the observations. Despite this, domains D4 and D1 simulated the offshore and onshore modes of rainfall somewhat satisfactorily. This hints that the west coast rainfall modes may not be as sensitive to the presence of the Western Ghats as previously assumed and are entirely driven by the large-scale variability, e.g., BSISO, as suggested by previous studies (Shige et al., 2017; Fletcher et al., 2020; Hunt et al., 2021). We explicitly show the influence of orography on the rainfall modes by performing a 'No orography' simulation (henceforth referred to as the *NoOrog* experiment) in which the Western Ghats are flattened entirely (Figure 1b). Note that the orography is flattened in all domains. Zhang and Smith (2018) performed a similar experiment in the WRF model and concluded that the offshore rainfall along the west coast was not caused by the orographic blocking from the Western Ghats. However, their focus was on the 'wet period' in which rainfall occurred onshore as well as offshore. Here, we focus on the offshore-onshore modes and the transition.

Zhang and Smith (2018) and Fletcher et al. (2020) emphasized the importance of offshore deep convection in suppressing rainfall over the west coast by cooling and drying the boundary layer. Domain D12 does not simulate the offshore heavy rainfall events probably due to the convective parameterization scheme. In the second experiment, we rerun the control simulation by turning off the convective parameterization scheme in D12 (henceforth referred to as the *NoCu* experiment). The aim of the second experiment is to check if explicit convection at 12-km horizontal grid spacing gives heavy rainfall and consequently, allows the west coast rainfall modes, and so whether the key difference between D12 and D4/D1 is the convective parameterization scheme rather than the resolution.

4.1 | Orography

Figures 12a-c show Hovmöller diagrams of 12-14°N averaged rainfall in the three domains for the *NoOrog* experiment. Note that the convective parameterization scheme in D12 is active in this experiment. Figures 12b,c show that the offshore rainfall mode is simulated in domains D4 and D1 even without the Western Ghats. The onshore rainfall is weak over the coast throughout the simulation. This is due to the absence of orographic uplifting. The offshore rainbands are practically unaffected by the removal of orography. Removal of the Western Ghats did not affect the diurnal cycle of rainfall either along the coast or in the offshore

region; we see early morning rainfall events in the *NoOrog* simulation quite similar to those when the orography was present (Fig. 2). This suggests that the land-sea contrast, more than the orography, affects the diurnal cycle of rainfall along the coast.

Figure 13 shows 850 hPa mean winds and geopotential field during the offshore and onshore modes for the *NoOrog* simulation. The evolution of large-scale fields is somewhat similar to the control run. During the offshore mode, a trough is present over the peninsula and the Arabian Sea, and during the onshore mode, an LPS has developed north of the Western Ghats. The winds are north-westerlies during the offshore mode, and during the onshore mode, they are stronger and westerly. Thus, the offshore and onshore modes of rainfall are linked to the evolution of the large-scale fields (as proposed by Shige et al. (2017); Fletcher et al. (2020); Hunt et al. (2021)). The Western Ghats merely modulate the intensity of rainfall over the coast through different orographic blocking regimes of the low-level flow which can be identified by classifying the onshore flow according to its Froude number as shown by Phadtare et al. (2022).

4.2 | Convective parameterization

In the *NoCu* experiment, the event was simulated employing only D12 but with explicit convection. Figure 12d shows a Hovmöller diagram of 12-14°N averaged rainfall for the *NoCu* experiment. It shows rainbands starting from the rain shadow region and propagating westwards over the Arabian Sea during 20-24 June. The intensity, as well as the organization of these rainfall episodes, seem abnormally high when compared with observations. This is an outcome of anomalously strong convection, possibly due to inadequate entrainment of dry air by the turbulent eddies into the convective core at 12 km horizontal grid spacing (Tang and Kirshbaum, 2020; Kirshbaum, 2020). The two modes seen in this experiment can be characterized as 'offshore propagation' and 'onshore propagation'. Offshore propagation of rainfall appears as one of the features of the offshore mode as it was seen in the other simulations (control and *NoOrog*) as well. Observations from IMERG suggest that a mixture of stationary and offshore-propagating rainfall episodes are present during the offshore mode. A trough present over the Indian peninsula and the Arabian Sea during the offshore mode might be promoting the westward propagation of rainfall. A similar phenomenon over the Indian region was noted by Phadtare and Bhat (2019) where deep clouds predominantly formed in the western flank of the trough and moved further westward.

In the *NoCu* experiment, the processes that suppress convection over the rain shadow region during the offshore mode are too weak or absent. Thus, convection gets triggered over the land during daytime due to the presence of the trough and moves westward with time. It arrives over the Arabian Sea during late-night to morning hours and further propagates offshore. On 25 June, there is a sudden change in the regime of rainfall formation and propagation. Hereafter, the storms form just off the coast and propagate onshore. The eastern limit of this propagation is set by the Western Ghats peak. Propagation of mesoscale systems depends on features such as downdrafts, cold pools, and gravity bores (Bukovsky et al., 2006), which are associated with heavily precipitating convective cores, or it can be a simple advection by the background flow. The former mechanism seems more likely during the offshore mode when the systems propagate upwind, while the latter is likely important during the onshore mode. It appears that as the explicit representation of convection simulates high-intensity rainfall, the aforementioned processes are stronger, which results in long-lasting (but constrained by the diurnal cycle) propagating mesoscale systems. With the convective scheme, rainfall intensities are weak and propagating systems are absent.

5 | CONCLUSIONS AND DISCUSSION

Simulations of the summer monsoon rainfall modes over the west coast of India were performed using the WRF model in order to understand the underlying mechanism driving these modes and the impacts of model resolution and the representation of convection on their simulation. It is concluded that the offshore and onshore rainfall modes are largely a consequence of

the large-scale atmospheric variability over this region. A schematic in Figure 14 summarizes the meteorological conditions controlling these rainfall modes. During the offshore mode, a trough extended over the Arabian Sea from the peninsula. It provided favourable conditions for offshore convection. As noted by Fletcher et al. (2020) in their observations, the low-level winds during this mode were weak. Shige et al. (2017) and Hunt et al. (2021) reported a positive vorticity anomaly over the offshore region during the offshore mode which is also a consequence of the trough. During the onshore mode, a ridge moved over the west coast and offshore region, which suppressed the large-scale convective activity over the offshore region. However, the low-level westerly winds were strong, resulting in the direct orographic uplift of winds and hence, heavy rainfall over the Western Ghats and west coast region. The following conclusions were drawn from the model simulations of this phenomenon performed in this study:

- **Orographic blocking**: The WRF model domains at 4- and 1.33-km grid spacing with explicit convection were able to simulate the broad features of the west coast rainfall modes. However, the coastal boundary layer in the model was too warm (by about 4-5 °C) and weakly stratified. This reduced the orographic blocking of the flow leading to an overestimation of the convective instability over the coast. As a result, there was anomalous deep convection and rainfall over the Western Ghats in the model simulations.
- **Diurnal cycle**: None of the domains simulated the observed diurnal cycle of rainfall over the west coast during the offshore mode correctly. All domains produced a daytime rainfall maximum over land which was not seen in the observations.
- **Convection scheme**: The model domain at 12-km horizontal resolution with a convection scheme could simulate the large-scale fields of the offshore and onshore modes but failed at simulating the rainfall modes associated with them. Convection, as well as rainfall intensity, in this domain, was very weak. On the other hand, turning off the convection scheme at this resolution resulted in an unrealistic overestimation of the rainfall intensity even over the rainshadow region.
- **Western Ghats**: The no-orography sensitivity experiment showed that the Western Ghats do not independently drive the offshore-onshore modes. However, they act as a barrier along the coast, keeping the rainfall predominantly offshore during the offshore mode. The coastal rainfall in the onshore mode is greatly enhanced due to the orographic uplifting.

Although the accuracy of IMERG rainfall can be questioned over the Western Ghats region, Flynn et al. (2017) reported that simulated rainfall over the west coast and Western Ghats was much greater in model simulations compared to their rain gauge observations. Given the uncertainties involved in model simulations, doubts can be raised regarding the pertinence of the conclusions of this study. Nevertheless, the rainfall accumulations in the offshore and onshore modes reported by Martin et al. (2020) (see figure 6 in that paper) in the MetUM are similar to those reported by the present study in Figure 4. Overestimation of orographic rainfall in the MetUM and other models based on the MetUM (e.g., NCUM) is also common (Martin et al., 2020). This suggests that the model biases reported here stem from the physics parameterization rather than the simulation uncertainties. Although this bias was blamed on the inadequate representation of convection in the models (Flynn et al., 2017), the simulated rainfall pattern in the present study is reminiscent of the idealized modelling experiments in which the Froude number of the flow was increased beyond 1 (Chu and Lin, 2000; Chen and Lin, 2005b,a; Jiang, 2003; Reeves and Lin, 2007; Miglietta and Rotunno, 2009). Our study points out that the underestimation of the orographic blocking by the model seems to be the primary cause behind it. The model does not adequately simulate the cold-air damming along the coast (Figs. 10 and 11), hence producing an anomalously warm and well-mixed PBL that weakens the orographic blocking by the Western Ghats. Although the model simulates the cold pools formed by the evaporation of rainfall (Fig. 7) and the temperature drop is also similar to that reported in observations by Fletcher et al. (2020) (figure 11b of that paper), the time scale for subsequent mixing and recovery of the PBL should be compared with the real world observations. In situ, high-resolution measurements on- and offshore are needed for this purpose.

Apart from the PBL scheme, the factors that can affect the structure of simulated PBL are the elevation of the lowest model

level and the number of levels within PBL. The lowest level in our simulations was at 20 m above the surface and there were 10 levels below 1500 m. Systematic model experiments can be performed to understand the sensitivity of these factors on the simulated PBL stratification. An underestimation low-level stratification can also result in reduced orographic drag in the upper atmosphere via weakened upward-propagating gravity waves (Wallace et al., 1983; Boer et al., 1984; Palmer et al., 1986; Bacmeister, 1993; Fritts and Alexander, 2003; Teixeira, 2014). This can have several consequences on the simulation of the Indian monsoon, including anomalously strong winds (Figure 6), stronger ventilation of the Indian peninsula by stronger winds, and hence, a weakened monsoon trough. Thus, in addition to the efforts of improving the representation of clouds and convection, land-atmosphere interaction, and aerosol effects, modelling of boundary layer processes and upscale propagation of orographic effects also needs attention in order to improve model simulations of the Indian monsoon.

REFERENCES

Bacmeister, J. T. (1993) Mountain-wave drag in the stratosphere and mesosphere inferred from observed winds and a simple mountain-wave parameterization scheme. *Journal of Atmospheric Sciences*, **50**, 377–399.

Birch, C., Webster, S., Peatman, S., Parker, D., Matthews, A., Li, Y. and Hassim, M. (2016) Scale interactions between the MJO and the western Maritime Continent. *Journal of Climate*, **29**, 2471–2492.

Birch, C. E., Roberts, M. J., Garcia-Carreras, L., Ackerley, D., Reeder, M. J., Lock, A. P. and Schiemann, R. (2015) Sea-breeze dynamics and convection initiation: The influence of convective parameterization in weather and climate model biases. *Journal of Climate*, **28**, 8093–8108.

Boer, G., McFarlane, N., Laprise, R., Henderson, J. and Blanchet, J.-P. (1984) The Canadian Climate Centre spectral atmospheric general circulation model. *Atmosphere-Ocean*, **22**, 397–429.

Bukovsky, M. S., Kain, J. S. and Baldwin, M. E. (2006) Bowing convective systems in a popular operational model: Are they for real? *Weather and forecasting*, **21**, 307–324.

Chen, F. and Dudhia, J. (2001) Coupling an advanced land surface–hydrology model with the Penn State–NCAR MM5 modeling system. Part I: Model implementation and sensitivity. *Monthly weather review*, **129**, 569–585.

Chen, S.-H. and Lin, Y.-L. (2005a) Effects of moist Froude number and CAPE on a conditionally unstable flow over a mesoscale mountain ridge. *Journal of the Atmospheric Sciences*, **62**, 331–350.

— (2005b) Orographic effects on a conditionally unstable flow over an idealized three-dimensional mesoscale mountain. *Meteorology and Atmospheric Physics*, **88**, 1–21.

Chen, Y., Chen, J., Chen, D., Xu, Z., Sheng, J. and Chen, F. (2021) A simulated radar reflectivity calculation method in numerical weather prediction models. *Weather and Forecasting*, **36**, 341–359.

Chu, C.-M. and Lin, Y.-L. (2000) Effects of orography on the generation and propagation of mesoscale convective systems in a two-dimensional conditionally unstable flow. *Journal of the Atmospheric Sciences*, **57**, 3817–3837.

Fletcher, J. K., Parker, D. J., Turner, A. G., Menon, A., Martin, G. M., Birch, C. E., Mitra, A. K., Mrudula, G., Hunt, K. M., Taylor, C. M. et al. (2020) The dynamic and thermodynamic structure of the monsoon over southern India: New observations from the INCOMPASS IOP. *Quarterly Journal of the Royal Meteorological Society*, **146**, 2867–2890.

Flynn, W. J., Nesbitt, S. W., Anders, A. M. and Garg, P. (2017) Mesoscale precipitation characteristics near the Western Ghats during the Indian Summer Monsoon as simulated by a high-resolution regional model. *Quarterly Journal of the Royal Meteorological Society*, **143**, 3070–3084.

Francis, P. and Gadgil, S. (2006) Intense rainfall events over the west coast of India. *Meteorology and Atmospheric Physics*, **94**, 27–42.

462 Fritts, D. C. and Alexander, M. J. (2003) Gravity wave dynamics and effects in the middle atmosphere. *Reviews of Geophysics*, **41**.

463 Gerard, L., Piriou, J.-M., Brožková, R., Geleyn, J.-F. and Banciu, D. (2009) Cloud and precipitation parameterization in a meso-gamma-
464 scale operational weather prediction model. *Monthly Weather Review*, **137**, 3960–3977.

465 Grossman, R. L. and Durran, D. R. (1984) Interaction of low-level flow with the Western Ghat mountains and offshore convection in the
466 summer monsoon. *Monthly Weather Review*, **112**, 652–672.

467 Hersbach, H., Bell, B., Berrisford, P., Biavati, G., Horányi, A., Muñoz Sabater, J., Nicolas, J., Peubey, C., Radu, R., Rozum, I. et al. (2018)
468 ERA5 hourly data on pressure levels from 1979 to present. *Copernicus Climate Change Service (C3S) Climate Data Store (CDS)*.
469 (Accessed on 12 NOV 2022), 10.24381/cds.bd0915c6.

470 Hong, S.-Y. and Lim, J.-O. J. (2006) The WRF single-moment 6-class microphysics scheme (WSM6). *Asia-Pacific Journal of Atmospheric*
471 *Sciences*, **42**, 129–151.

472 Hong, S.-Y., Noh, Y. and Dudhia, J. (2006) A new vertical diffusion package with an explicit treatment of entrainment processes. *Monthly*
473 *Weather Review*, **134**, 2318–2341.

474 Honnert, R. (2016) Representation of the grey zone of turbulence in the atmospheric boundary layer. *Advances in Science and Research*,
475 **13**, 63–67.

476 Huffman, G. J., Bolvin, D. T., Nelkin, E. J. and Tan, J. (2015) Integrated Multi-satellitE Retrievals for GPM (IMERG) technical
477 documentation. *NASA/GSFC Code*, **612**, 2019.

478 Hunt, K. M. and Menon, A. (2020) The 2018 Kerala floods: A climate change perspective. *Climate Dynamics*, **54**, 2433–2446.

479 Hunt, K. M., Turner, A. G., Stein, T. H., Fletcher, J. K. and Schiemann, R. K. (2021) Modes of coastal precipitation over southwest India
480 and their relationship with intraseasonal variability. *Quarterly Journal of the Royal Meteorological Society*, **147**, 181–201.

481 Iacono, M. J., Delamere, J. S., Mlawer, E. J., Shephard, M. W., Clough, S. A. and Collins, W. D. (2008) Radiative forcing by long-lived
482 greenhouse gases: Calculations with the AER radiative transfer models. *Journal of Geophysical Research: Atmospheres*, **113**.

483 Jiang, Q. (2003) Moist dynamics and orographic precipitation. *Tellus A: Dynamic Meteorology and Oceanography*, **55**, 301–316.

484 Kirshbaum, D. J. (2020) Numerical simulations of orographic convection across multiple gray zones. *Journal of the Atmospheric Sciences*,
485 **77**, 3301–3320.

486 Kirshbaum, D. J., Adler, B., Kalthoff, N., Barthlott, C. and Serafin, S. (2018) Moist orographic convection: Physical mechanisms and
487 links to surface-exchange processes. *Atmosphere*, **9**, 80.

488 Krishnan, R., Zhang, C. and Sugi, M. (2000) Dynamics of breaks in the Indian summer monsoon. *Journal of the atmospheric sciences*,
489 **57**, 1354–1372.

490 Kumar, A., Dudhia, J., Rotunno, R., Niyogi, D. and Mohanty, U. (2008) Analysis of the 26 July 2005 heavy rain event over Mumbai, India
491 using the Weather Research and Forecasting (WRF) model. *Quarterly Journal of the Royal Meteorological Society*, **134**, 1897–1910.

492 Kumar, S. and Bhat, G. (2017) Vertical structure of orographic precipitating clouds observed over south Asia during summer monsoon
493 season. *Journal of Earth System Science*, **126**, 1–12.

494 Mahoney, K. M. (2016) The representation of cumulus convection in high-resolution simulations of the 2013 Colorado Front Range flood.
495 *Monthly Weather Review*, **144**, 4265–4278.

496 Martin, G. M., Brooks, M. E., Johnson, B., Milton, S. F., Webster, S., Jayakumar, A., Mitra, A. K., Rajan, D. and Hunt, K. M. (2020)
497 Forecasting the monsoon on daily to seasonal time-scales in support of a field campaign. *Quarterly Journal of the Royal Meteorological*
498 *Society*, **146**, 2906–2927.

Miglietta, M. M. and Rotunno, R. (2009) Numerical simulations of conditionally unstable flows over a mountain ridge. *Journal of the Atmospheric Sciences*, **66**, 1865–1885.

Mohandas, S., Francis, T., Singh, V., Jayakumar, A., George, J. P., Sandeep, A., Xavier, P. and Rajagopal, E. (2020) NWP perspective of the extreme precipitation and flood event in Kerala (India) during August 2018. *Dynamics of Atmospheres and Oceans*, **91**, 101158.

Murali Krishna, U., Das, S. K., Deshpande, S. M., Doiphode, S. and Pandithurai, G. (2017) The assessment of Global Precipitation Measurement estimates over the Indian subcontinent. *Earth and Space Science*, **4**, 540–553.

Palmer, T., Shutts, G. and Swinbank, R. (1986) Alleviation of a systematic westerly bias in general circulation and numerical weather prediction models through an orographic gravity wave drag parametrization. *Quarterly Journal of the Royal Meteorological Society*, **112**, 1001–1039.

Peatman, S. C., Matthews, A. J. and Stevens, D. P. (2014) Propagation of the Madden–Julian Oscillation through the Maritime Continent and scale interaction with the diurnal cycle of precipitation. *Quarterly Journal of the Royal Meteorological Society*, **140**, 814–825.

Phadtare, J. (2018) Role of Eastern Ghats orography and cold pool in an extreme rainfall event over Chennai on 1 December 2015. *Monthly Weather Review*, **146**, 943–965.

Phadtare, J. and Bhat, G. (2019) Characteristics of deep cloud systems under weak and strong synoptic forcing during the Indian summer monsoon season. *Monthly Weather Review*, **147**, 3741–3758.

Phadtare, J. A., Fletcher, J. K., Ross, A. N., Turner, A. G. and Schiemann, R. K. (2022) Froude number-based Rainfall Regimes over the Western Ghats Mountains of India. *Quarterly Journal of the Royal Meteorological Society*.

Prakash, S. and Srinivasan, J. (2021) A comprehensive evaluation of near-real-time and research products of IMERG precipitation over India for the southwest monsoon period. *Remote Sensing*, **13**, 3676.

Rajendran, K., Kitoh, A., Srinivasan, J., Mizuta, R. and Krishnan, R. (2012) Monsoon circulation interaction with Western Ghats orography under changing climate. *Theoretical and Applied Climatology*, **110**, 555–571.

Reeves, H. D. and Lin, Y.-L. (2007) The effects of a mountain on the propagation of a preexisting convective system for blocked and unblocked flow regimes. *Journal of the Atmospheric Sciences*, **64**, 2401–2421.

Rojas, Y., Minder, J. R., Campbell, L. S., Massmann, A. and Garreaud, R. (2021) Assessment of GPM IMERG satellite precipitation estimation and its dependence on microphysical rain regimes over the mountains of south-central Chile. *Atmospheric Research*, **253**, 105454.

Saha, U., Gupta, M. D. and Mitra, A. K. (2021) Monitoring the Quality of AWS/ARG Rainfall Observations over India during Monsoon Season. Available at `https://www.ncmrwf.gov.in/Reports-eng/Report_AWS_ARG_Feb_2021_Final_Upal_Saha_NCMRWF.pdf`.

Sheppard, P. (1956) Airflow over mountains. *Quarterly Journal of the Royal Meteorological Society*, **82**, 528–529.

Shige, S., Nakano, Y. and Yamamoto, M. K. (2017) Role of orography, diurnal cycle, and intraseasonal oscillation in summer monsoon rainfall over the Western Ghats and Myanmar Coast. *Journal of Climate*, **30**, 9365–9381.

Shrestha, D., Deshar, R. and Nakamura, K. (2015) Characteristics of summer precipitation around the Western Ghats and the Myanmar West Coast. *International Journal of Atmospheric Sciences*, **2015**.

Skamarock, W. C., Klemp, J. B., Dudhia, J., Gill, D. O., Barker, D. M., Wang, W. and Powers, J. G. (2008) A description of the advanced research WRF version 3. *Tech. rep.*, University Corporation for Atmospheric Research.

Smith, R. B. (1979) The influence of mountains on the atmosphere. In *Advances in Geophysics*, vol. 21, 87–230. Elsevier.

Smith, S., Vosper, S. and Field, P. (2015) Sensitivity of orographic precipitation enhancement to horizontal resolution in the operational Met Office Weather forecasts. *Meteorological Applications*, **22**, 14–24.

Stensrud, D. J. (2009) *Parameterization schemes: keys to understanding numerical weather prediction models*. Cambridge University Press.

Tang, S. L. and Kirshbaum, D. (2020) On the sensitivity of deep-convection initiation to horizontal grid resolution. *Quarterly Journal of the Royal Meteorological Society*, **146**, 1085–1105.

Teixeira, M. A. (2014) The physics of orographic gravity wave drag. *Frontiers in Physics*, **2**, 43.

Tiedtke, M. (1989) A comprehensive mass flux scheme for cumulus parameterization in large-scale models. *Monthly Weather Review*, **117**, 1779–1800.

Turner, A. G., Bhat, G., Martin, G., Parker, D. J., Taylor, C., Mitra, A. K., Tripathi, S. N., Milton, S., Rajagopal, E., Evans, J. G. et al. (2020) Interaction of convective organization with monsoon precipitation, atmosphere, surface and sea: The 2016 INCOMPASS field campaign in India. *Quarterly Journal of the Royal Meteorological Society*, **146**, 2828–2852.

Wallace, J. M., Tibaldi, S. and Simmons, A. J. (1983) Reduction of systematic forecast errors in the ECMWF model through the introduction of an envelope orography. *Quarterly Journal of the Royal Meteorological Society*, **109**, 683–717.

Wyngaard, J. C. (2004) Toward numerical modeling in the "Terra Incognita". *Journal of the Atmospheric Sciences*, **61**, 1816–1826.

Xu, W. and Rutledge, S. A. (2015) Morphology, intensity, and rainfall production of MJO convection: Observations from DYNAMO shipborne radar and TRMM. *Journal of the Atmospheric Sciences*, **72**, 623–640.

Zhang, C., Wang, Y. and Hamilton, K. (2011) Improved representation of boundary layer clouds over the southeast Pacific in ARW-WRF using a modified Tiedtke cumulus parameterization scheme. *Monthly Weather Review*, **139**, 3489–3513.

Zhang, D. and Anthes, R. A. (1982) A high-resolution model of the planetary boundary layer—Sensitivity tests and comparisons with SESAME-79 data. *Journal of Applied Meteorology (1962-1982)*, 1594–1609.

Zhang, G. and Smith, R. B. (2018) Numerical study of physical processes controlling summer precipitation over the Western Ghats region. *Journal of Climate*, **31**, 3099–3115.

Zheng, Y., Alapaty, K., Herwehe, J. A., Del Genio, A. D. and Niyogi, D. (2016) Improving high-resolution weather forecasts using the Weather Research and Forecasting (WRF) Model with an updated Kain–Fritsch scheme. *Monthly Weather Review*, **144**, 833–860.

6 | ACKNOWLEDGEMENTS

This work and its contributors (JAP, JKF, ANR, AGT, RKHS, HLB) were funded through the Weather and Climate Science for Service Partnership (WCSSP) India, a collaborative initiative between the Met Office, supported by the UK Government's Newton Fund, and the Indian Ministry of Earth Sciences (MoES). This work was undertaken on ARC4, part of the High Performance Computing facilities at the University of Leeds, UK. The ERA5 data was obtained via the Climate Data Store (CDS). JAP thanks Thorwald H.M. Stein and Kieran M.R. Hunt at the University of Reading and A. Jayakumar at the National Centre for Medium Range Weather Forecasting (NCMRWF) for their constructive comments on this study.

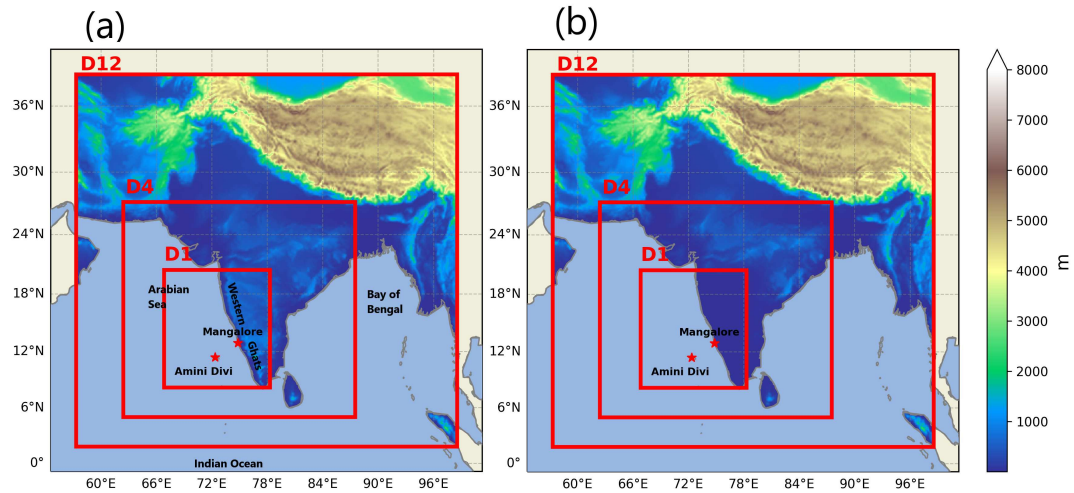

FIGURE 1 Model domains and orography for (a) Control run, and (b) *NoOrog* run described in section 4.1. Grid spacings: D12 - 12 km, D4 - 4 km, and D1 - 1.33 km.

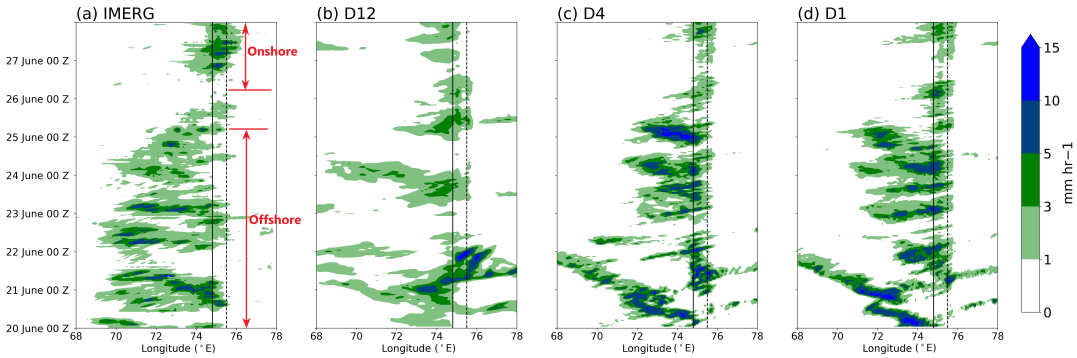

FIGURE 2 Hovmöller plot of 12-14°N averaged rainfall in (a) IMERG, (b) D12, (c) D4, and (d) D1 during 20-27 June 2016. The solid black line shows the mean longitude of the coast and the dotted line shows the mean longitude of the Western Ghats peak between 12-14°N.

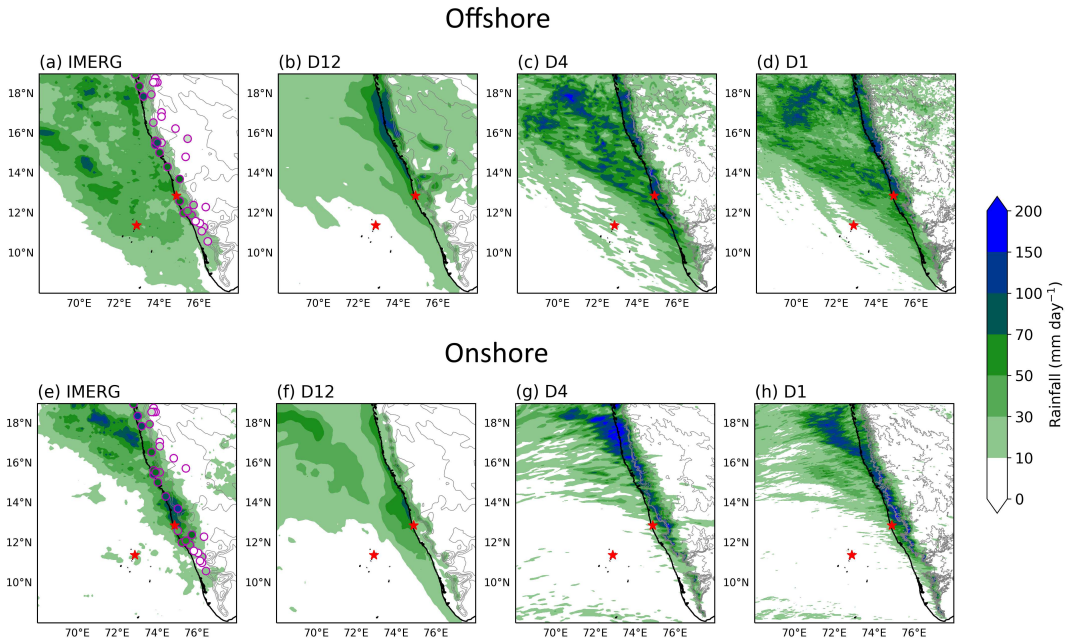

FIGURE 3 Mean rainfall during the offshore mode (20-24 June) in (a) IMERG, (b) D12, (c) D4, and (d) D1. (e)-(g) are the same as (a)-(d), respectively, but for the onshore mode (26-27 June). The stars show the locations of Mangalore (coast) and Amini Divi (island) stations. The circles along the west coast in (a) and (e) show the locations of rain gauges from which data is used and their face colours show the mean rainfall recorded by them during respective modes.

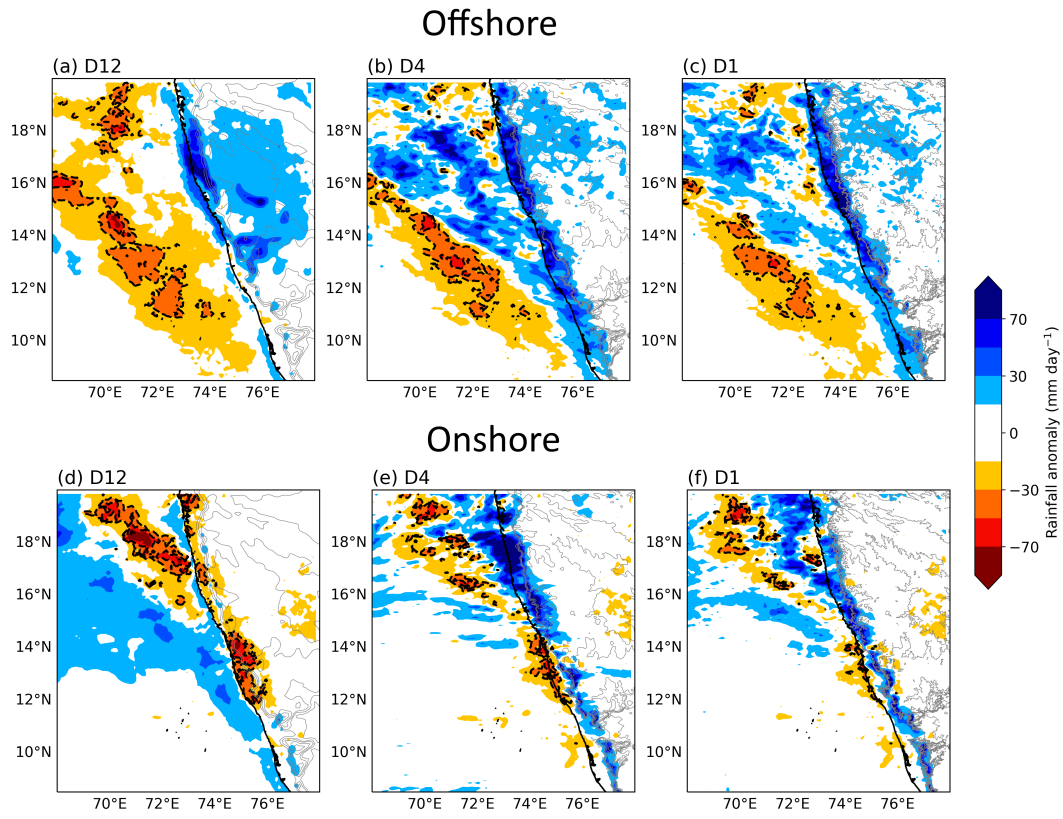

FIGURE 4 Rainfall anomaly in (a) D12, (b) D4, and (c) D1 with respect to the IMERG rainfall during the offshore mode. (d)-(f) Same as (a)-(c), respectively, but during the onshore mode.

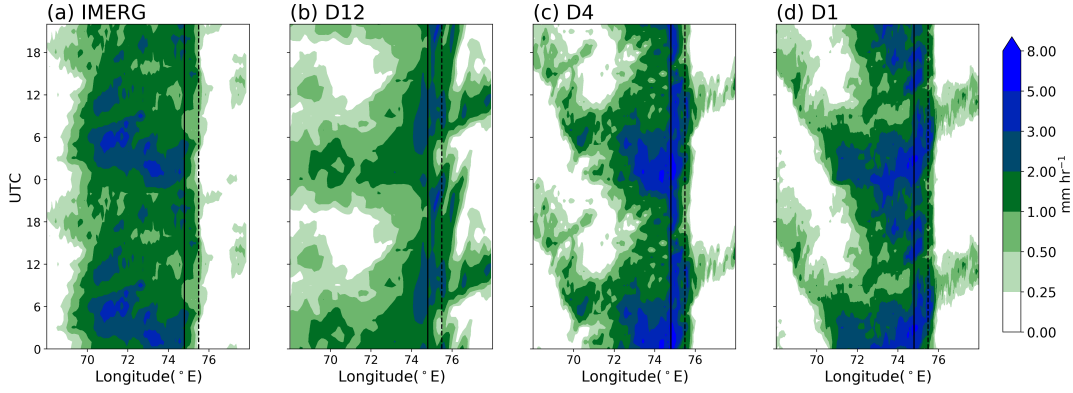

FIGURE 5 Diurnal variation of mean rainfall over 12-14°N band in (a) IMERG, (b) D12, (c) D4, and (d) D1 during the offshore mode.

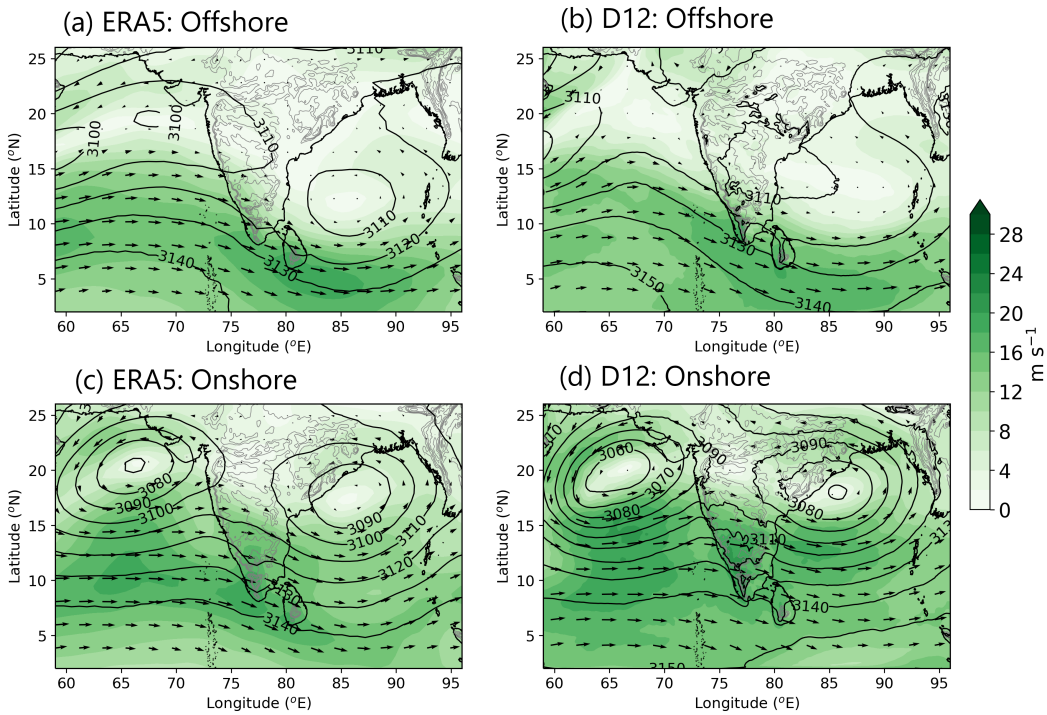

FIGURE 6 Mean 700 hPa geopotential height (m) contours and wind speed (shading) from (a) ERA5 and (b) D12 during the offshore mode. (c),(d) same as (a),(b) but for the onshore mode.

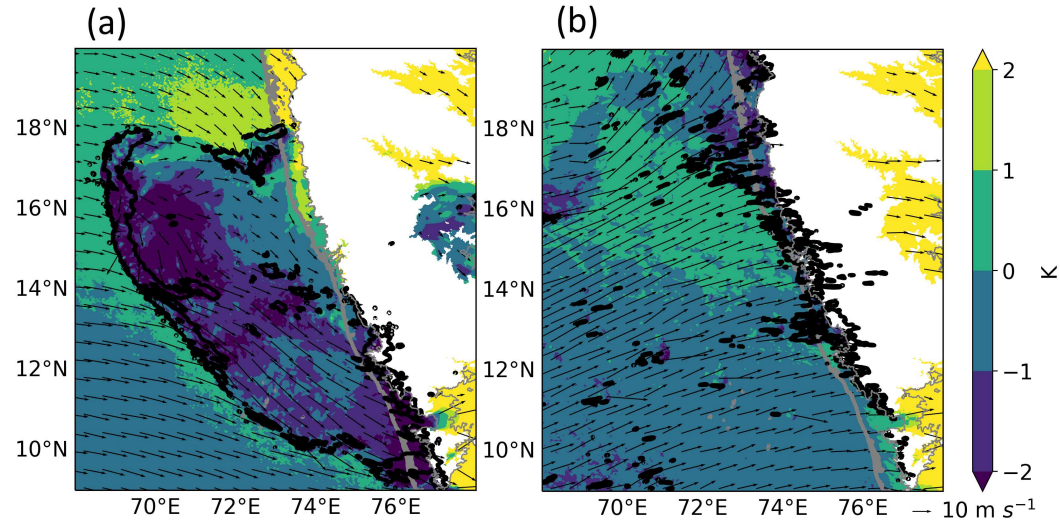

FIGURE 7 Virtual potential temperature perturbation (shading) and winds at 950 hPa in D1 at (a) 0500 UTC 20 June (offshore mode) and (b) 0500 UTC 27 June (onshore mode); The black contours delineate regions where rainfall $\geq$ 5 mm hr^{-1}.

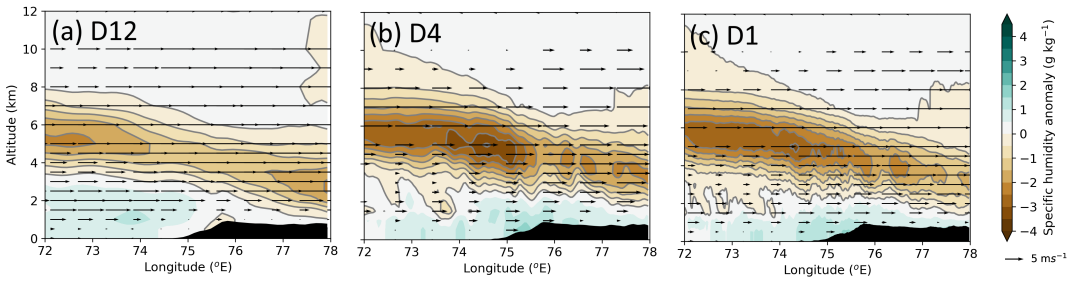

FIGURE 8 Difference between the mean zonal winds (vectors) and specific humidity (shading) over the 12-14°N band during the onshore and offshore modes (onshore-offshore) simulated by (a) D12, (b) D4 and (c) D1. The grey contours delineate negative anomalies of the specific humidity.

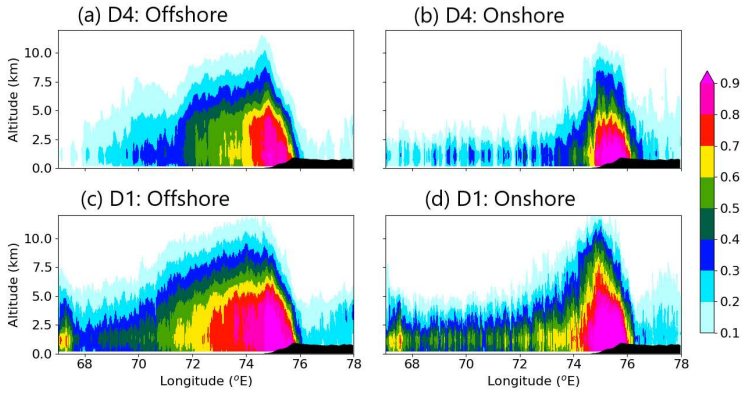

FIGURE 9 Temporal fraction for which the simulated radar reflectivity was $\geq$ 20 dBZ in at least one grid box in the 12-14°N band in D4 during the (a) offshore and (b) onshore modes. (c)-(d) are same as (a)-(b), respectively, but for the D1 domain.

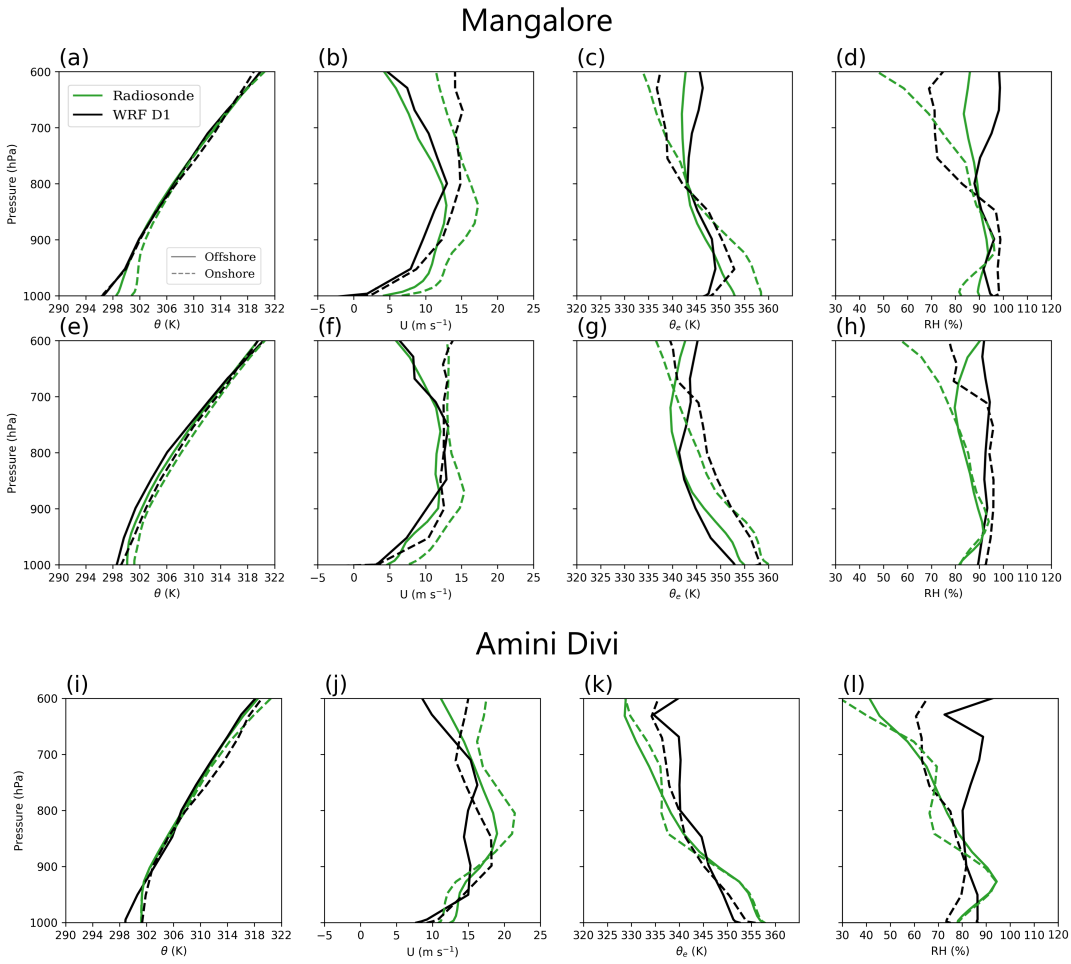

FIGURE 10 Mean vertical profiles of (a) Potential temperature (θ), (b) zonal winds (U), (c) equivalent potential temperature (θ_e), and (d) relative humidity during the offshore and onshore modes from the 0000 UTC Mangalore (a coastal station) radiosondes and the corresponding simulated soundings in D1. (e)-(h) are the same as (a)-(d) but for the 1200 UTC radiosondes. (i)-(l) are the same as (a)-(d) but for the 0000 UTC Amini Divi (an island station) radiosondes. The simulated profiles are averaged over a 12 km box centred over the sounding location.

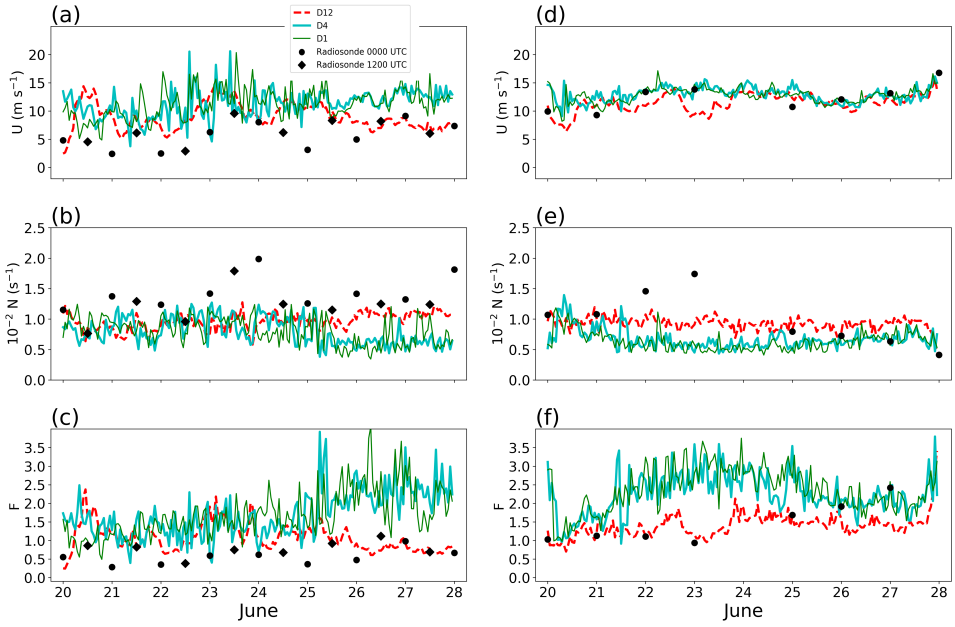

FIGURE 11 Mean values of (a) Zonal winds (U), (b) Brunt-Väisälä frequency (N), and (c) Froude number (F) over the 50-1000 m layer calculated from the 0000 and 1200 UTC Mangalore (a coastal station) radiosonde soundings and the hourly simulated soundings in the three WRF grids (D12, D4, and D1) over the same location as Mangalore. (d)-(f) are same as (a)-(c) but for the Amini Divi (an island station) radiosonde soundings.

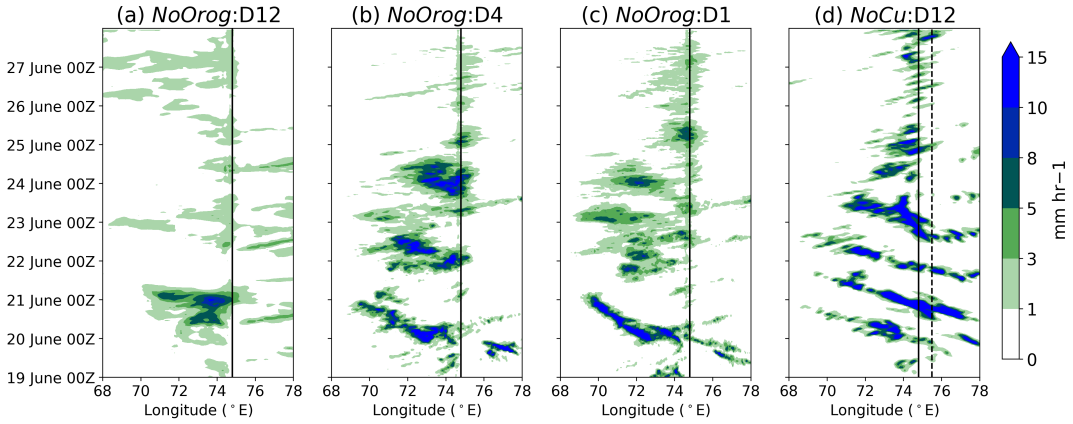

FIGURE 12 Hovmöller plot of 12-14°N averaged rainfall in (a) D12, (b) D4, and (c) D1 from the *NoOrog* simulation. (d) Same as (a) but for the *NoCu* simulation. The solid black line shows the mean longitude of the coast and the dotted line shows the mean longitude of the Western Ghats peak between 12-14°N.

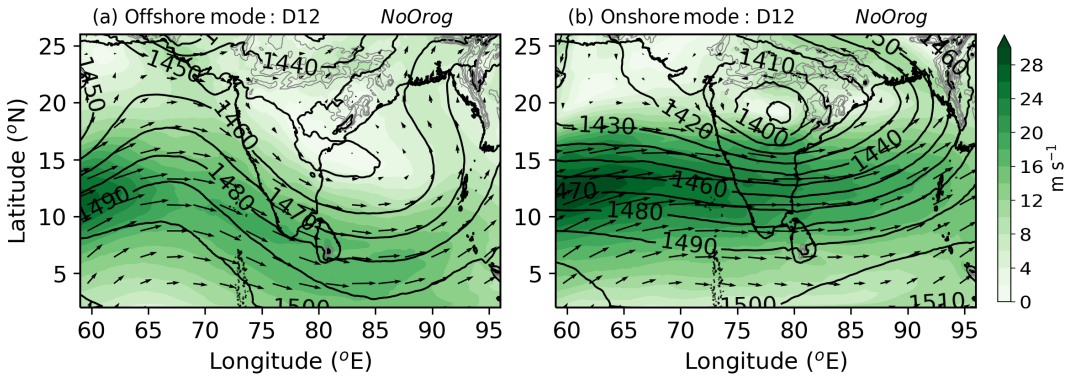

FIGURE 13 Mean 850 hPa geopotential height (m) contours and wind speed (shading) during the (a) offshore and (b) onshore modes in the D12 domain from the *NoOrog* simulation.

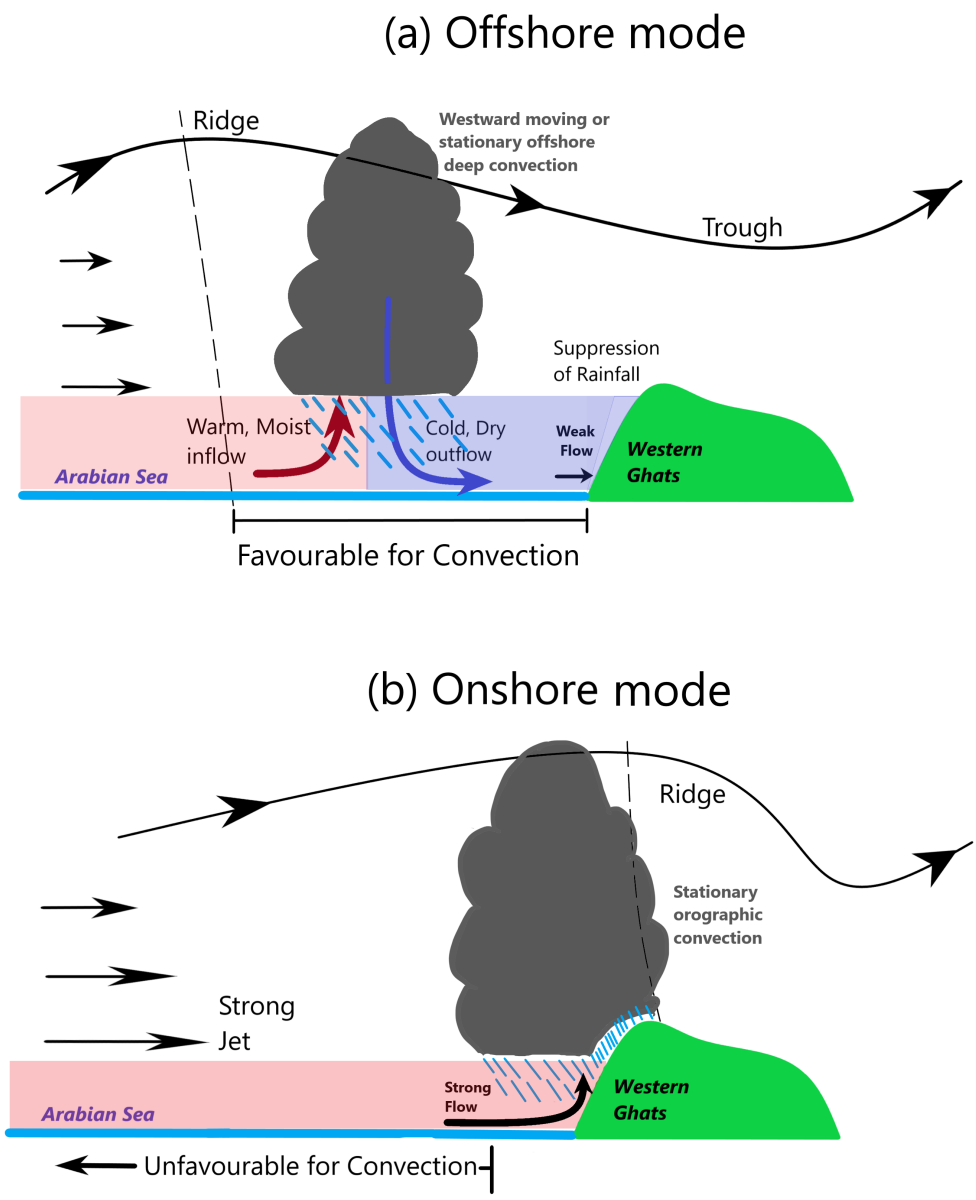

FIGURE 14 Schematics of the (a) offshore and (b) onshore rainfall modes over the west coast of India. An offshore trough facilities offshore convection and rainfall over the Arabian Sea. The cold and dry outflows from the offshore rainfall suppress rainfall over the Western Ghats. During onshore mode, a ridge over the coast suppresses offshore rainfall. Westerlies are stronger during this phase and enhanced rainfall over the coast and Western Ghats results from the orographic uplifting.